ANCHORAGE AND BOND BEHAVIOUR OF NEAR SURFACE MOUNTED CARBON FIBRE REINFORCED POLYMER BARS

Perera W.K.K.G.
Department of Architecture and Civil Engineering, University of Bath, Bath, BA2 7AY, UK

Ibell T.J.
Department of Architecture and Civil Engineering, University of Bath, Bath, BA2 7AY, UK

Darby A.P.
Department of Architecture and Civil Engineering, University of Bath, Bath, BA2 7AY, UK

Denton S.R.
Parsons Brinckerhoff, Queen Victoria House, Redland Hill, Bristol, BS6 6US, UK

Abstract

The use of the Near Surface Mounted (NSM) Fibre Reinforced Polymer (FRP) bars to retrofit existing concrete structures is now mainstream, with many examples across the world. This strengthening technique offers many advantages over the external bonding of FRP plates or sheets, particularly with respect to bond properties and durability. However, successful application of the technique relies on the knowledge of anchorage length requirements for each NSM FRP bar. This paper presents the details and the results of a series of experiments investigating the bond behaviour between NSM CFRP bars and concrete considering the effect of several parameters; bond length, bar size, surface texture of the bar, slot size and concrete strength. The effect of the investigated variables on bond behaviour is discussed in detail along with the modes of failure. Analysis of the results including strain, slip and bond stress distributions along the bond length are presented, with a focus on the local bond stress-slip relationship. The proposed bond strength and corresponding slip values in the present study are found to be comparable with the ones found in literature.

INTRODUCTION

Recently, the NSM FRP technique has emerged as a more effective strengthening technique than the Externally Bonded Reinforcement (EBR) FRP technique in many instances because of its ability to gain higher bond strengths and the possibility of precluding or delaying premature debonding failures, which are often observed with the externally bonded reinforcement [1]. The NSM FRP technique involves bonding FRP bars into pre-cut grooves on the concrete cover of a structural member to be strengthened, using an adhesive. The application of the NSM technique covers both reinforced and prestressed concrete structures as well as structures made of other materials, such as timber and masonry. Although, a limited number of research studies on NSM systems is currently available, the research carried out so far indicates that the NSM technique is a promising and effective technique in increasing both flexural and shear capacities of structural members such as beams [2, 3, 4, 5].

The bond which transfers the stresses between the FRP reinforcement and concrete is of prime importance in order to form the composite action of a composite structural member. Several research studies have been reported on the investigation of bond behaviour between NSM FRP reinforcements and concrete [2, 6, 7, 8, 9, 10, 11, 12, 13, 14]. In these studies, the effects of various parameters including the bond length have been considered. Successful application of this technique is highly dependent on the anchorage length (or the development length), the length a reinforcing bar can resist a tensile force equal to its ultimate tensile strength. Most of the existing anchorage models for NSM FRP bars are based on limited test data and are dependent on the type, size and shape of the reinforcement used, and the test conditions of the particular research study. In other words, they are empirical and can only be applied to specific situations. Therefore, it is required that a generalised model which captures the mechanics of the bond behaviour be developed.

There are several possible failure mechanisms which may lead to anchorage failure of a NSM FRP-to-concrete bonded joint namely; rupture of the bar, slip of the bar through the resin (failure at the bar-resin interface), failure in shear of the resin which can normally be avoided if the shear strength of the resin is comparatively high, resin splitting due to high tensile radial stresses, failure at the resin-concrete interface or failure of the concrete itself. The effects of several parameters; bond length, bar size, surface texture of the bar, slot size and concrete strength, on bond behaviour between NSM CFRP reinforcements and concrete have been investigated in the research presented in this paper. The paper describes tests and analysis which have been conducted on this topic, with the aim of producing a comprehensive set of design criteria for the prediction of bond capacity in the anchorage zone of round NSM CFRP bars.

TEST PROGRAM

The experimental program consists of 6 series, each composed of four bond specimens, investigating the effect of bond length, bar size, surface texture of the bar, groove size and concrete strength on bond between NSM CFRP bars and concrete. The bond specimens were of 110 mmx220 mm in cross section and 750 mm long. The test setup and the reinforcement details are shown in figure 1. The specimen was of easily manageable size and since the specimen was tested vertically, it was possible to visually inspect the bonded joint while loading progressed. Further, the specimen configuration allowed monitoring of both the loaded and free end slips. The bond specimen was designed in such a way that it will not fail in shear, flexure or compression before the bond failure occurs. The amount of flexural steel reinforcement was selected to avoid any flexural failure before the bond failure occurs and also to resemble the percentage of the internal steel reinforcement in practical situations.

Table 1 summarises the details of 24 bond specimens that were tested. Bond lengths of 40, 20, 10 and 5 times the bar diameter and two nominal compressive strengths of concrete; 30 N/mm^2 and 60 N/mm^2, were considered. Two bar diameters; 9 mm and 12 mm, and two types of CFRP bars with different surface textures; CARBOPREE and ASLAN 200 manufactured by Sireg, Italy and Hughes Brothers, USA, respectively, were used. The groove size was classified as small/large depending on how large it was compared to the bar diameter. When the groove dimension (the groove width and depth were the same because all the grooves were square in cross section) was 4 mm wider than the bar diameter, it was regarded as ‘small’ and when the groove dimension was 8 mm wider than the bar diameter it was classified as ‘large’. The designations of the specimens are of the form of “series number_ bar

diameter_ bar type (A-Aslan/ C-Carbopree) _nominal compressive strength of concrete_ size of the groove (S-small/ L-large) _bond length (in terms of number of bar diameters)".

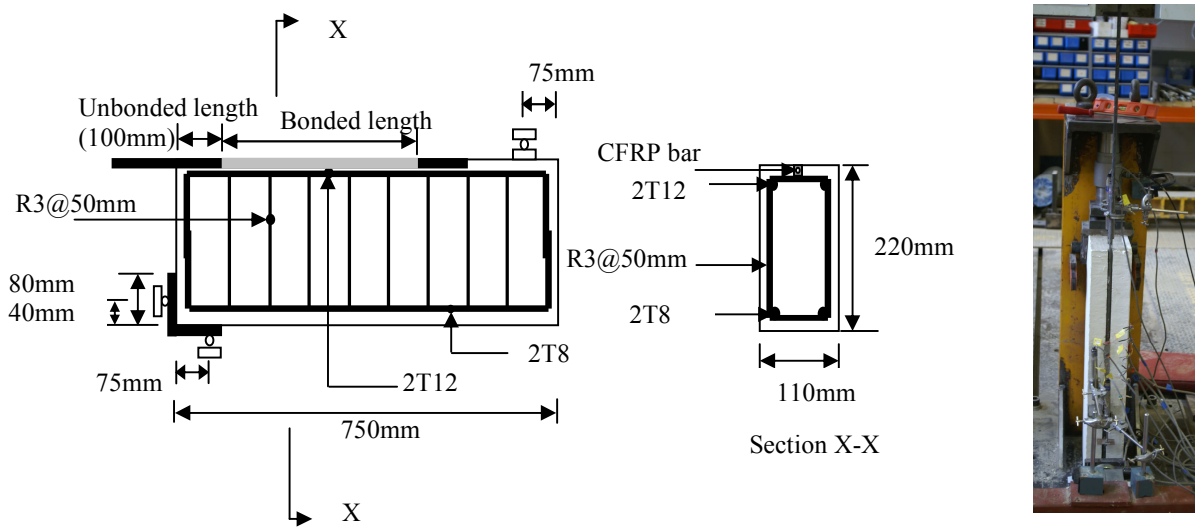

Figure 1: Test setup

Concrete cubes of 100 mm were cast from each concrete mix and the actual compressive strength of concrete was determined by the average compressive strength of three or more cubes. 150 mm diameter 300 mm long cylinders were used to obtain the splitting tensile strength of the concrete. The tensile strength and the modulus of elasticity of CARBOPREE bars were 2300 MPa and 130 GPa respectively, and that of ASLAN 200 bars were 2068 MPa and 124 GPa respectively, as provided by the manufacturers. Steel rebars of 12 mm were used as the flexural reinforcement, and 8 mm steel rebars were used in the compression zone. The shear stirrups were of 3 mm mild steel. According to the tensile tests performed, the average ultimate strength of the mild steel was 658 N/mm^2. The adhesive used was a high modulus, high strength two part structural epoxy paste (Sikadur 30). According to the manufacturer's specifications, the tensile strength and the Young's modulus of the adhesive were 24.8 MPa and 4.48 GPa, respectively.

The strain distribution along the bonded length was monitored by number of strain gauges, whose gauge length was 6mm, located on the bar surface within the bonded length, while one strain gauge was positioned in the unbonded region. The CFRP bar with strain gauges was placed in the groove as in figure 2, in order to minimize the disturbance from the strain gauges to the bond action. The CFRP bar was gripped to the machine jaws, by placing two 2 mm thick aluminium tabs in between the bar and the jaws, in order to prevent premature failure of the bar at the grips. The load was applied by a universal testing machine with a capacity of 2000 kN, at a cross head displacement rate of 0.5 mm/min. A Linear Variable Displacement Transducer (LVDT) was attached to the bar, at a known distance from the loaded end (l/e) to measure the l/e slip. At the free end (f/e), two LVDTs, whose readings were taken to calculate the f/e slip, were placed to measure the displacements of the concrete and the bar. The external compressive force and the reaction of the bottom support were monitored by the load cells of 500 kN and 200 kN respectively.

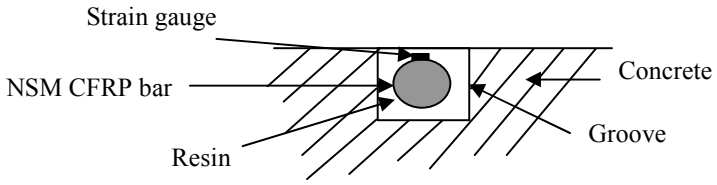

Figure 2: Alignment of the CFRP bar with strain gauges

Table 1: Specimen details; N/A – not available

	Specimen designation	Bar diameter (mm)	Bond length (number of bar diameters)	Groove size (width/ depth) (mm)	Young's modulus of bars (experimental) (GPa)	Nominal compressive strength of concrete (MPa)	Actual compressive strength of concrete (MPa)	Splitting tensile strength of concrete (MPa)
Series 1	1_12_C_60_S_40	12	40	16	150	60	62.11	N/A
	1_12_C_60_S_20		20				58.30	2.80
	1_12_C_60_S_10		10				58.30	2.80
	1_12_C_60_S_5		5				58.30	2.80
Series 2	2_9_A_60_L_40	9	40	18	129	60	53.88	2.30
	2_9_A_60_L_20		20				53.54	3.00
	2_9_A_60_L_10		10				53.88	2.30
	2_9_A_60_L_5		5				53.88	2.30
Series 3	3_12_A_60_S_40	12	40	16	130	60	55.87	2.97
	3_12_A_60_S_20		20				55.87	2.97
	3_12_A_60_S_10		10				53.54	3.00
	3_12_A_60_S_5		5				53.54	3.00
Series 4	4_9_A_60_S_40	9	40	13	130	60	56.95	2.80
	4_9_A_60_S_20		20				56.95	2.80
	4_9_A_60_S_10		10				55.87	2.97
	4_9_A_60_S_5		5				56.95	2.80
Series 5	5_12_C_30_S_40	12	40	16	150	30	34.98	2.20
	5_12_C_30_S_20		20				33.73	2.20
	5_12_C_30_S_10		10				33.73	2.20
	5_12_C_30_S_5		5				33.73	2.20
Series 6	6_9_A_30_S_40	9	40	13	130	30	34.98	2.20
	6_9_A_30_S_20		20				34.98	2.20
	6_9_A_30_S_10		10				34.98	2.20
	6_9_A_30_S_5		5				33.73	2.20

TEST RESULTS

Table 2 summarises the main results obtained.

Failure Modes

Five types of failure modes; failure at the bar-resin interface (pull out failure), failure at the resin-concrete interface, catastrophic failure in the concrete, cracking of the concrete surrounding the groove with the resin being intact and splitting of the resin cover, were identified (figure 3). The splitting of the resin cover can be further categorised into four modes; longitudinal resin splitting with almost no or slight damage in the surrounding concrete, longitudinal resin splitting accompanied by cracking of the surrounding concrete, longitudinal and transverse resin splitting with no damage to the concrete and longitudinal and transverse resin splitting accompanied by cracking of the concrete. The splitting of the resin cover was the most common and the dominant mode of failure among the other failure modes, which resulted due to excessive tensile stresses of the resin cover. A common feature to most of the tested specimens was the formation of a crack at the f/e (Refer figure 3 (a), (c) and (h)). Sometimes, there were few shear cracks in some specimens running deeper into the beam up to the level of internal steel reinforcement.

Table 2: Test results

	Specimen designation	Ultimate load (kN)	(Ultimate load/ ultimate strength of the bar)%	Average bond strength (MPa)	Mode of failure
Series 1	1_12_C_60_S_40	70.81	27.23	3.91	Resin splitting
	1_12_C_60_S_20	57.81	22.23	6.39	Resin splitting
	1_12_C_60_S_10	32.90	12.65	7.27	Resin splitting
	1_12_C_60_S_5	21.98	8.45	9.72	Failure at the bar-resin interface
Series 2	2_9_A_60_L_40	78.99	58.58	7.76	Catastrophic failure in the concrete
	2_9_A_60_L_20	58.17	43.15	11.43	Catastrophic failure in the concrete
	2_9_A_60_L_10	34.86	25.85	13.70	Resin splitting
	2_9_A_60_L_5	19.11	14.17	15.02	Resin splitting
Series 3	3_12_A_60_S_40	76.00	33.93	4.20	Catastrophic failure in the concrete
	3_12_A_60_S_20	70.50	31.48	7.79	Resin splitting
	3_12_A_60_S_10	46.94	20.96	10.38	Resin splitting
	3_12_A_60_S_5	26.13	11.67	11.55	Failure at the resin-concrete interface
Series 4	4_9_A_60_S_40	68.37	50.71	6.72	Resin splitting
	4_9_A_60_S_20	48.83	36.22	9.60	Premature failure at the grips
	4_9_A_60_S_10	32.96	24.45	12.95	Resin splitting
	4_9_A_60_S_5	21.61	16.03	16.98	Resin splitting
Series 5	5_12_C_30_S_40	69.04	26.55	3.82	Catastrophic failure in the concrete
	5_12_C_30_S_20	66.23	25.47	7.32	Failure at the resin-concrete interface
	5_12_C_30_S_10	37.30	14.35	8.24	Resin splitting
	5_12_C_30_S_5	28.63	11.01	12.66	Cracking of the concrete with no damage in the resin cover
Series 6	6_9_A_30_S_40	50.73	37.62	4.98	Catastrophic failure in the concrete
	6_9_A_30_S_20	44.81	33.23	8.80	Resin splitting
	6_9_A_30_S_10	27.59	20.46	10.84	Cracking of the concrete with no damage in the resin cover
	6_9_A_30_S_5	20.14	14.94	15.83	Cracking of the concrete with no damage in the resin cover

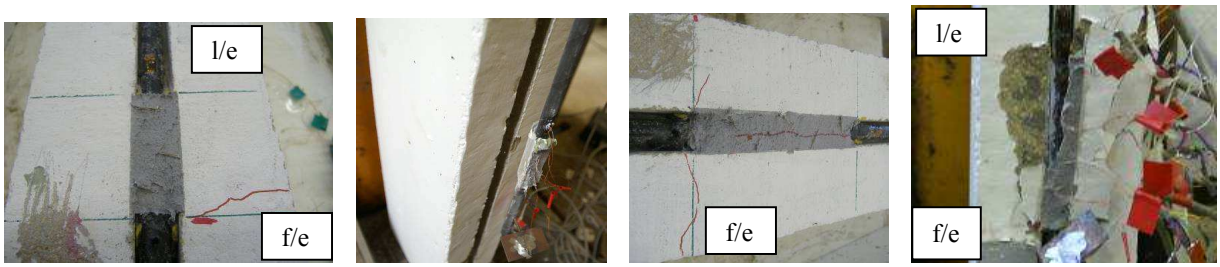

(a) (b) (c) (d)

Figure 3: Failure modes; (a) bar-resin interface failure (pull out failure), (b) resin-concrete interface failure, (c) longitudinal resin splitting with slight damage in the surrounding concrete, (d) longitudinal resin splitting accompanied by cracking of the surrounding concrete, (e) longitudinal and transverse resin splitting accompanied by cracking of the concrete, (f) catastrophic failure in the concrete, (g) cracking of the concrete surrounding the groove with the resin being intact and (h) longitudinal and transverse resin splitting with almost no cracking in the concrete

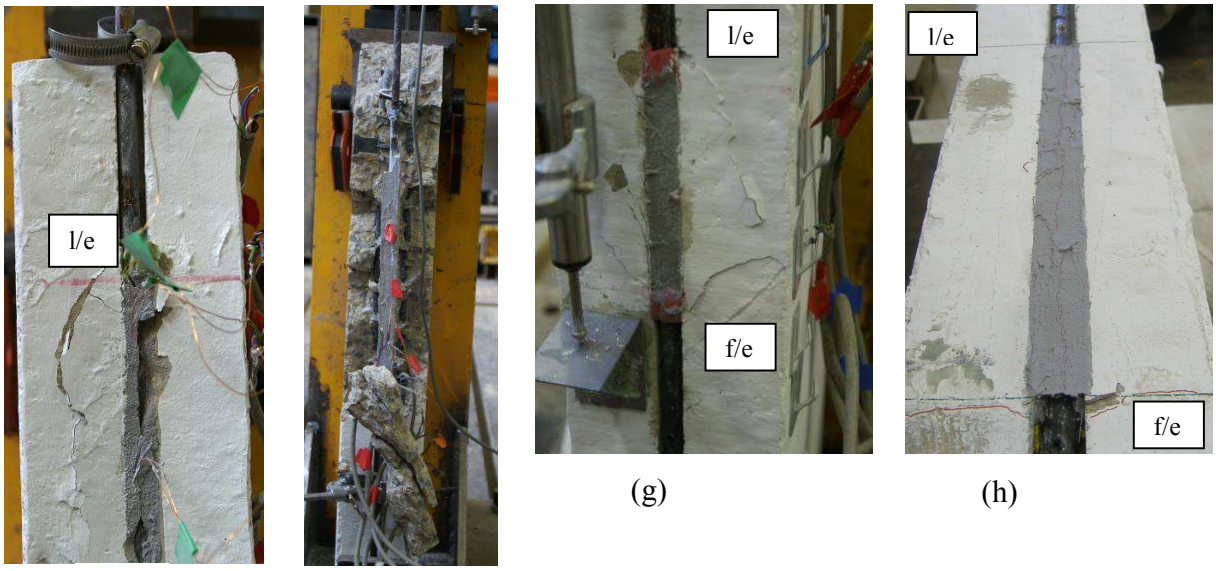

(e) (f) (g) (h)

Figure 3: Contd.

Effect of the test variables

Figure 4(a) shows that the ultimate load increases as the bond length increases up to a value corresponding to a certain value of the bond length, after which the ultimate load seems to remain constant for further increments of the bond length. This trend is clearly visible in series 1, 3, 5 and 6. In the case of series 2 and 4, it was not clear enough to make a judgement because the mode of failure of specimen 2_9_A_60_L_20 (catastrophic failure in the concrete) was different to those of the other series, and the corresponding specimen in series 4, specimen 4_9_A_60_S_20, was unable to give a consistent value by failing prematurely at the grips. Figure 4(b) represents the relationship between the average bond strength and the bond length. It seems that the average bond strength decreases as the bond length increases. It is clearly because the ultimate load is not proportional to the bond length. The rate of decrease in the average bond strength with the increase in bond length, seems to be more or less the same for Aslan 200 bars of both 9 mm and 12 mm diameters, irrespective of the other variables (series 2, 3, 4 and 6).

The comparison of series 2 and 4 implies the effect of groove size on bond behaviour. The mechanics of cover splitting bond failure of a NSM FRP- concrete bonded joint is similar to that of a deformed steel bar in concrete [15]. The radial component of bond stresses induces hoop tensile stresses in the resin cover, which may lead to longitudinal splitting of the resin cover once the tensile strength of the resin is exceeded. Therefore, resin cover splitting failure depends on the thickness of the resin cover and the tensile strength of the resin. When the groove size increased in series 2, the thickness of the resin cover also increased so that the resistance to splitting of the resin cover increased, and the ultimate load increased correspondingly as well. There was a marginal difference between the ultimate loads of the specimens with a bond length of 5 times the bar diameter (5d) (specimens 2_9_A_60_L_5 and 4_9_A_60_L_5), for the increment in the resin cover thickness. The maximum percentage of increase in the ultimate load (15.5%) could be observed between specimens 2_9_A_60_L_40 and 4_9_A_60_S_40, which had the longest bond length (40d), and the change of the resin cover thickness has influenced the mode of failure of those specimens. Specimen 4_ 9_A_60_S_40 with the small groove size, failed by longitudinal and transverse splitting of the resin cover followed by cracking of the surrounding concrete (figure 3(e)), whereas specimen 2_9_A_60_L_40, with the large groove size, failed catastrophically in the concrete (figure 3(f)). Furthermore, the latter had the highest ultimate load recorded within the whole test program. The increase in the resin cover thickness was able to prevent resin cover splitting failure so that failure occurred in the adjacent concrete.

Series 4 and 6 compare the effect of the concrete strength on bond behaviour of Aslan bars, and series 1 and 5 compare that of Carbopree bars. The effect of the concrete strength on the ultimate load seems to be dependent on type of the bar because for Aslan 200 bars, the ultimate load tends to increase as the concrete strength increases,

whereas the ultimate load of Carbopree bars seems to decrease with the increase in concrete strength. The highest percentage of increase in the ultimate load could be seen for the specimen with the longest bond length, and the highest percentage of decrease in the ultimate load was for the specimen with the shortest bond length, as can be seen in figure 4(c). The average percentage of increase in the ultimate load was 7%, for Aslan bars, and the average percentage of decrease in the ultimate load was 11%, for Carbopree bars. Presently, it is not possible to make a final conclusion about the effect of the concrete strength on the ultimate load, since more tests should be conducted to plot more consistent curves. Series 3 and 4 compare the specimens with different sizes of bars, and show that the specimens with 12 mm bars could reach higher ultimate loads than those with 9 mm bars.

There is a noticeable difference between the ultimate loads and the failure modes of the specimens in series 1 and 3, due to the difference in the surface texture of the bars. Aslan 200 bars could develop a stronger bond than Carbopree bars, so that the ultimate loads of the specimens with Aslan bars with bond lengths of 40d, 20d, 10d and 5d, had an increase of 7.3%, 22%, 42.7% and 18.9%, respectively, compared to those of Carbopree bars. The pull-out failure was observed only in a specimen with Carbopree bars (specimen 1_12_C_60_S_5). Specimen 1_12_C_60_S_5 failed at the bar-resin interface, indicating that the surface texture of the bar was not able to provide enough mechanical interlocking to resist bond stresses. The surface deformations of Aslan bars were able to create a sound bond between the bar and the resin, so that failure occurred either in the resin cover or the concrete.

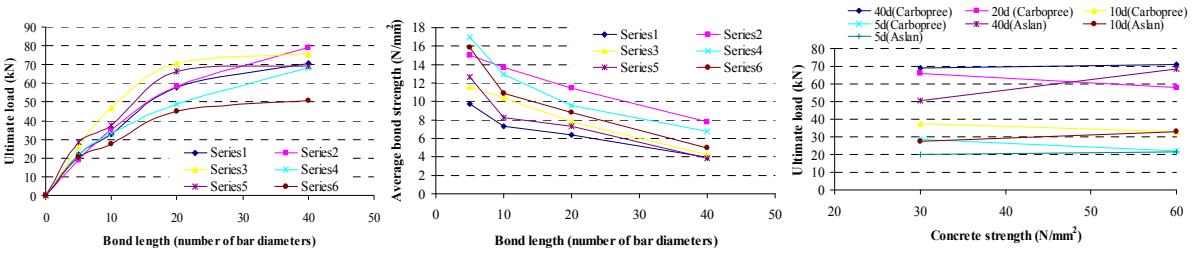

Figure 4: (a) Ultimate load vs. bond length, (b) average bond strength vs. bond length and (c) ultimate load vs. concrete strength

ANALYSIS OF RESULTS

Local bond stress-slip relationship

The local bond stress, slip distributions were obtained by analysing the strain gauge readings and the measured free end slip as explained by De Lorenzis and Nanni [6], by considering the equilibrium of a part of the CFRP bar with a small length, *dx* and assuming linear elastic behaviour of the bar. Thus, the local bond stress, $\tau(x)$ is given by;

$$\tau(x) = \frac{d_f E_f d\epsilon_f(x)}{4 \quad dx} \tag{1}$$

where x= coordinate along the bond length starting from the free end, d_f = diameter of the bar, E_f = Young's modulus of the bar and $\epsilon_f(x)$ = axial strain of the bar. The local slip of the bar along the bond length is given by;

$$s(x) = s_{fe} + \int_0^x \epsilon_f(x)\, dx \tag{2}$$

where s_{fe} is the free end slip. The strain versus location graphs were plotted for different load levels as a percentage of the ultimate load, assuming that the strain at the free end is zero. The local bond stress and slip distributions along the bond length at different load levels were also obtained, by approximating the equations (1) and (2) for discrete

stain gauge readings [6]. Finally, the bond stress versus location and the slip versus location data were combined to plot the bond stress versus slip curves at the each strain gauge location.

Figure 5 depicts the strain, bond stress and slip distributions for two specimens, specimen 4_9_A_60_S_40 and specimen 6_9_A_30_S_5 at different load levels, as a percentage of the ultimate load. Specimen 4_9_A_60_S_40 represents the general behaviour of all the specimens with the longest bond length (40d), and specimen 6_9_A_30_S_5 illustrates the common behaviour of the specimens with the shortest bonded length (5d), irrespective of the other variables. There is a clear difference between the behaviour of the specimens with long bond lengths and that with short bond lengths. The strain distribution of specimen 4_9_A_60_S_40 is generally non linear at low load levels, and tends to follow a linear shape as the load approaches the ultimate, whereas that of specimen 6_9_A_30_S_5 shows some linearity even at low load levels. It seems that the bond stresses tend to become more even at final load levels in the specimens with long bond lengths, due to the redistribution of bond stresses after micro cracking at the l/e. The approximate linearity of the strain distribution, even at low load levels, suggests that the bond stresses are always constant along the bond length, in the specimens with short bond lengths. Further, in the specimens with short bond lengths, there are gradual strain increments for all the load increments (or almost equal strain increments for equal load increments), at all strain gauge locations unlike in the case with the specimens with long bond lengths, where the largest increment of strain always occurs for the final load increment (90-100%).

At low load levels, in specimen 4_9_A_60_S_40, the bond stress at the free end is almost zero and at the ultimate load level it increases considerably, showing that the whole bond length contributes to the bond action as the load increases. Initially, only a part of the bond length, which is close by to the loaded end, is resisting the pulling action, and once the bond resistance is lost there, the other part of the bond length starts resisting the applied load, thereby increasing the bond stresses at the free end. This is clearly indicated by the peak value moving towards the free end, and by the bond stress at the loaded end decreasing, during the final load levels. This phenomenon is completely different for the specimens with short bond lengths, where the bond stress at the free end gradually increases from the beginning of the load application. That means, the whole bond length of the specimens with short bond lengths, is contributing to the bond resistance from the start to the end of the pull-out action. The free end slip of the specimens with long bond lengths is almost zero at low load levels. The specimens with short bond lengths show an almost constant slip distribution along the whole bond length, at all load levels. Even at low load levels, the free end slip of those specimens is comparatively higher than that of the specimens with long bond lengths. As the load increases, the gradual slip increments can be seen accordingly in those specimens, unlike in the case with the specimens with long bond lengths.

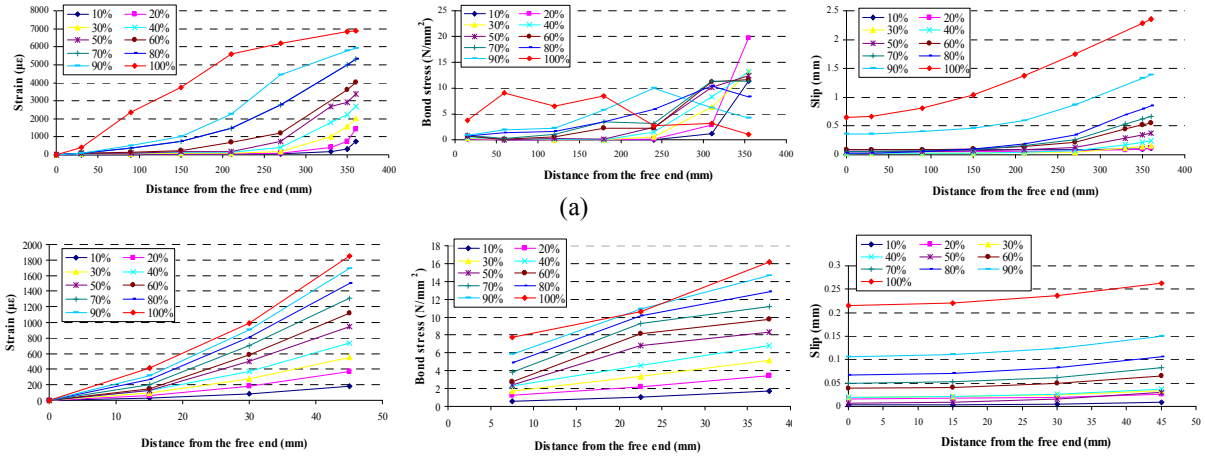

(a)

(b)

Figure 5: Strain, bond stress and slip distributions along the bond length; (a) specimen 4_9_A_60_S_40, (b) specimen 6_9_A_30_S_5

Figure 6 illustrates the bond stress versus slip distribution at the location of each strain gauge along the bond length, for specimen 4_9_A_60_S_40 and specimen 6_9_A_30_S_5, which represent the general bond-slip behaviour of the specimens tested with, the longest bond length and the shortest bond length, respectively. These graphs are obtained from the bond stress and slip values at each load level up to the ultimate load level. In other words, the bond-slip behaviour at the each strain gauge location, only up to the ultimate load level is considered. The bond-slip relationships are quite irregular because both the bond stress and the slip values are based on a limited number of strain gauge readings, and affected by imperfections in the interface conditions. In spite of the irregularity, the basic shape of the bond-slip curve is clearly visible in both graphs. Since the f/e slip readings of specimen 4_9_A_60_S_40 were highly irregular during the initial stages of loading, the bond-slip curves at the locations closer to the free end (for example, the 15 mm, 60mm and 120mm locations) have been affected significantly by that. Therefore, the bond-slip curves at those locations show a significant deviation from the desired shape of the bond-slip curve, whereas this effect is marginal on the bond-slip curves at the locations away from the f/e.

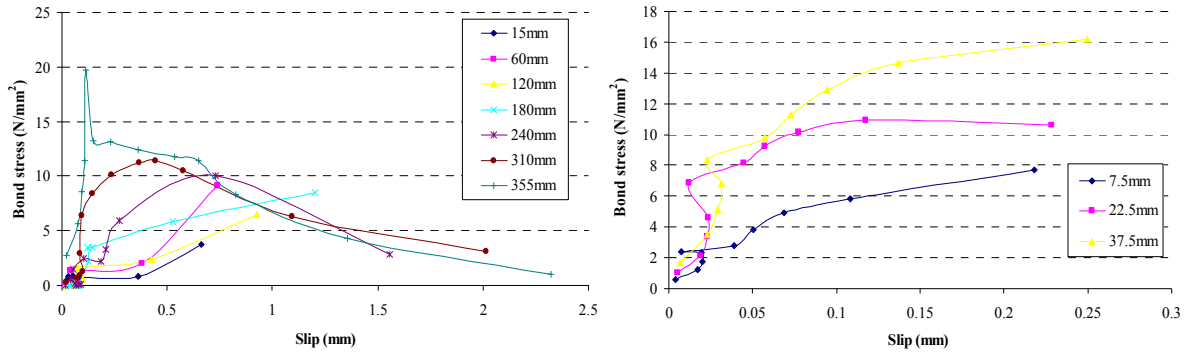

(a) (b)

Figure 6: Bond-slip curves; (a) specimen 4_9_A_60_S_40, (b) specimen 6_9_A_30_S_5

The main difference between the shapes of the two graphs is that there is no post peak branch for the specimens with short bond lengths, because the bond length is not long enough for the redistribution of bond stresses to occur by the time the ultimate load is reached, unlike in the case with the specimens with long bond lengths. Further, there is a significant difference between the bond behaviour at the 15mm location of specimen 4_9_A_60_S_40 and the 7.5mm location of specimen 6_9_A_30_S_5. The 15mm location, being the closest point to the free end of specimen 4_9_A_60_S_40, has not reached the peak bond stress at all. The 7.5mm location, being the closest point to the free end of specimen 6_9_A_30_S_5 has almost reached the peak value, and behaves almost the same as the other points along the same specimen, confirming that the whole bond length of the specimens with short bond lengths contributes to the bond resistance from the very beginning to the end of the pull-out action. Despite the large scatter of plotted points, one can suggest a peak bond stress between 12 and 13 MPa, corresponding to a slip value between 0.2 and 0.35 for specimen 4_9_A_60_S_40, and a peak bond stress around 14 MPa, and a corresponding slip value around 0.25 for specimen 6_9_A_30_S_5. The comparison of the values proposed here, particularly the slip values corresponding to the maximum bond stress, with the ones found in the literature [12, 16], reveals that these values are fairly comparable, and confirms the general bond behaviour of NSM CFRP bars. On the other hand, the validity of a direct comparison is doubtful since the materials and the shapes of the bars used are different.

CONCLUSIONS

Different types of failure modes namely, failure at the bar-resin interface, failure at the resin-concrete interface, catastrophic failure in the concrete, cracking of the concrete surrounding the groove with the resin cover being intact and splitting of the resin cover, were identified. The effect of the investigated parameters on bond behaviour between NSM CFRP bars and concrete can be listed briefly as follows. The ultimate load increased as the bond length increased up to a value corresponding to a certain value of the bond length, after which the ultimate load seemed to remain constant for further increments of the bond length. As the groove size increased so the ultimate load increased. The effect of the concrete strength on the ultimate load seemed to be dependent on the type of the

bar used. The ultimate load could be increased by increasing the bar diameter. The overall bond performance of Aslan bars was better than that of Carbopree bars, indicating that the surface texture of the bar has a great influence on the bond behaviour. The slip and bond stress distributions along the bonded joint seem to be nearly constant for short bond lengths, at any given load level, unlike in the case with long bond lengths. The observed bond strength and corresponding slip values are within the range of the values found by the other researchers.

It is scheduled to conduct similar experimental studies with two other shapes of CFRP bars, rectangular and square, so that the effect of bar shape on bond behaviour between NSM CFRP bars and concrete, can be investigated. Further, it is intended to develop an analytical model based on fracture mechanics, which captures the failure behaviour realistically to predict the bond failure load and the anchorage length of NSM CFRP bars.

REFERENCES

1. Hassan T and Rizkalla S, "Investigation of Bond in Concrete Structures Strengthened with Near Surface Mounted Carbon Fibre Reinforced Polymer Strips", *Journal of Composites for Construction*, 7(3), pp 248-257, 2003.
2. Hassan T and Rizkalla S, "Bond Mechanism of Near Surface Mounted Fibre Reinforced Polymer Bars for Flexural Strengthening of Concrete Structures", *ACI Structural Journal*, 101(6), pp 830-839, 2004.
3. Nanni A, Di Ludovico M and Parretti R, "Shear Strengthening of a PC Bridge Girder with NSM CFRP Rectangular Bars", *Advances in Structural Engineering*, 7(4), pp 97-109, 2004.
4. De Lorenzis L and Nanni A, "Shear Strengthening of Reinforced Concrete Beams with Near Surface Mounted Fibre Reinforced Polymer Rods", *ACI Structural Journal*, 98(1), pp 60-68, 2001.
5. De Lorenzis L and Nanni A, "Characterization FRP Rods as Near Surface Mounted Reinforcement", *Journal of Composites*, 5(2), pp 114-121, 2001.
6. De Lorenzis L and Nanni A, "Bond Between Near Surface Mounted Fibre Reinforced Polymer Rods and Concrete in Structural Engineering", *ACI Structural Journal*, 99(2), pp 123-132, 2002.
7. Hassan T, Mohamedien M, Hassan N and Rizkalla S, "Bond Performance of Different FRP Strengthening Systems", *Engineering Research Journal*, 5(2), pp 15-23, 2001.
8. Yan X, Miller B, Nanni A and Bakis C E, "Characterization of CFRP Rods Used as Near Surface Mounted Reinforcement", Proc., 8th International Structural Faults and Repair Conf., Forde M C, Ed., Engineering Technics Press, Edinburgh, Scotland, CD-ROM, 1999.
9. Shield C, French C and Milde E "The Effect of Adhesive Type on the Bond of NSM Tape to Concrete", Proc., 7th International Symposium on Non-Metallic FRP Reinforcement for Concrete Structures (FRPRCS-7), Kansas City, USA, pp 355-372, 2005.
10. Blaschko M and Zilch K, "Rehabilitation of Concrete Structures with CFRP Strips Glued into Slits", Proc., 12th International Conference on Composite Materials, Organization of the Int. Conf. on Composite Materials, Paris, CD-ROM, 1999.
11. Carolin A, Nordin H and Taljsten B, "Concrete beams strengthened with near surface mounted reinforcement of CFRP", Proc., International Conference on FRP Composites in Civil Engineering, Research Centre for Advanced Technology in Structural Engineering, Dept. of Civil and Structural Engineering, Hong Kong Polytechnic University, Hong Kong, pp 1059-1066, 2001.
12. Teng J G, De Lorenzis L, Wang B, Li R, Wong T N and Lam L, "Debonding Failures of RC Beams Strengthened with Near Surface Mounted CFRP Strips", *Journal of Composites for Construction*, 10(2), pp 92-105, 2006.
13. Sena Cruz J M, "Strengthening of Concrete Structures with Near Surface Mounted CFRP Laminate Strips", PhD Thesis, Dept. of Civil Engineering, University of Minho, Portugal, 2004.
14. De Lorenzis L, "Strengthening of RC Structures with Near Surface Mounted FRP Rods", PhD Thesis, Dept. of Innovation Engineering, University of Leece, Italy, 2002.
15. De Lorenzis L and Teng J G, "Near Surface Mounted FRP Reinforcement: An Emerging Technique for Strengthening Structures", *Composites:Part B*, 38(2007), pp 119-143, 2007.
16. Sena Cruz J M and Barros J A O, "Modelling of Bond between Near Surface Mounted CFRP Laminate Strips and Concrete", *Computers and Structures*, 82(17-19), pp 1513-1521, 2004.